POLITECNICO DI TORINO
Repository ISTITUZIONALE

An analysis of the PM10 chemical composition and its spatial and seasonal variation in Piedmont (Italy) using Raman spectroscopy

(Article begins on next page)

22 December 2024

An analysis of the PM$_{10}$ chemical composition and its spatial and seasonal variation in Piedmont (Italy) using Raman spectroscopy

Lia Drudi [a,*], Matteo Giardino [b,c], Marilena Tedone [a], Andrea Tiano [c], Davide Janner [c,d], Federica Pognant [e], Francesco Matera [e], Milena Sacco [f], Luisella Bardi [f], Rossana Bellopede [a]

[a] Department of Environment, Land and Infrastructure Engineering (DIATI), Politecnico di Torino, Corso Duca degli Abruzzi 24, 10129 Torino, Italy
[b] Department of Applied Science and Technology (DISAT), Politecnico di Torino, Viale Teresa Michel 5, 15121 Alessandria, Italy
[c] Department of Applied Science and Technology (DISAT), Politecnico di Torino, Corso Duca degli Abruzzi 24, 10129 Torino, Italy
[d] INSTM, Consorzio Interuniversitario Nazionale per la Scienza e Tecnologia dei Materiali, Via G. Giusti 9, 50121 Firenze, Italy
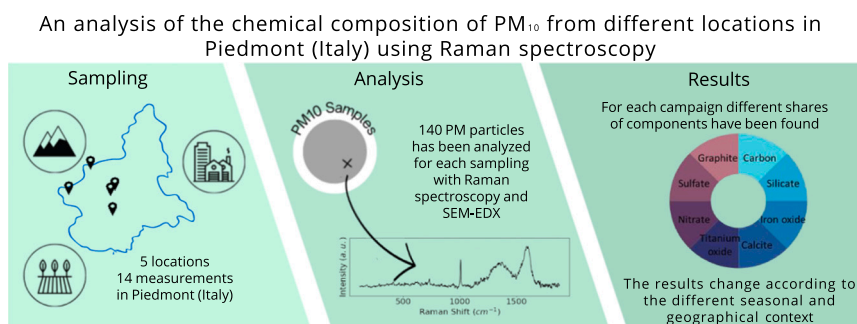[e] Evironment Direction, Regione Piemonte, Via Principe Amedeo, Torino, Italy
[f] Arpa Piemonte, Via PO VII, Torino, Italy

HIGHLIGHTS

- The study utilizes Raman spectroscopy to analyze the chemical composition of PM10.
- PM samples come from different anthropic contexts (urban, suburban and rural).
- Raman spectroscopy identified significant composition differences.
- The composition changes greatly according to the season and geographical context.

GRAPHICAL ABSTRACT

An analysis of the chemical composition of PM$_{10}$ from different locations in Piedmont (Italy) using Raman spectroscopy

ABSTRACT

Particulate Matter (PM) dramatically affects the well-being of a growing global population, particularly in urban areas. While air quality control is an important and pressing issue, particulate matter analysis typically focuses on size distribution and concentration, offering limited insights into chemical composition and pollutant sources.

This study analyzes PM$_{10}$ samples collected from five air quality monitoring stations across the Piedmont region. Specifically, the two of the stations are located in the urban environment of Turin, a city known as one of Europe's most polluted cities. The analysis has been carried out using primarily Raman Spectroscopy (RS) to identify the main PM components, investigate the different PM compositions, and evaluate the chemical and seasonal variations. Scanning Electron Microscopy (SEM) equipped with an Energy Dispersion X-ray spectrophotometer (EDX) has also been used to obtain further information about the elemental composition and the size distribution.

Amorphous carbon, nitrate salt, sulfate salt, iron oxides, and quartz are the main compounds found. The results of our study highlight significant differences in the chemical composition of PM$_{10}$, indicating variations in the sources and characteristics of PM. Notably, higher levels of nitrate and sulfate particles are linked

respectively to cold and warm seasons. Whereas, amorphous carbon and iron oxides are associated with distinct geographic features at the sampling sites, such as traffic conditions. These findings emphasize the importance of understanding the different sources and characteristics of PM_{10} to develop effective air pollution mitigation strategies in the Piedmont region.

1. Introduction

Globally, atmospheric aerosols substantially impact human health, air quality, and climate. In particular, the light-scattering properties of atmospheric aerosols cause collateral damage to visibility and climate (Seinfeld and Pandis, 2006; Sobanska et al., 2014). On the other hand, the size, chemical composition, and mass concentration of PM particles determine their adverse effects on human health. Fine particles can penetrate the human respiratory system through the trachea and bronchi, while ultrafine particles can pass through the alveolar epithelium and enter the bloodstream directly after inhalation (Kampa and Castanas, 2008; Schwartz, 2004; Schwarze et al., 2006). Since PM is also composed of a wide diverse range of chemical species, its chemical composition is crucial in determining whether exposure to pollutants will have a detrimental impact on human health and providing accurate information for identifying various emission sources. Information concerning chemical heterogeneity is essential to understanding and predicting the impacts of PM in terms of reactivity, environmental impact, and human health (Manisalidis et al., 2020; Morakinyo et al., 2016; Yang et al., 2018).

In this work, the PM characterization is carried out using Raman and SEM-EDX spectroscopy to obtain complementary information. Raman spectroscopy is a non-invasive and non-destructive technique widely used for the rapid investigation of atmospheric aerosol particles (Doughty and Hill, 2020; Estefany et al., 2023; Liang et al., 2022; Sobanska et al., 2014). Specifically, each molecular species exhibits a characteristic "fingerprint" Raman spectrum, providing an unambiguous identification of typical aerosol particles by their distinctive peaks in the Raman spectra (Doughty and Hill, 2020; Liang et al., 2022).

On the other hand, it can only detect functional groups that are Raman-active and to determine the exact molecular structure, further analytical techniques are needed (Liang et al., 2022). Furthermore, some PM components can cause a strong fluorescence that interferes with the peak identification in the Raman spectra (Liang et al., 2022). In addition, if the PM compound is composed of more than one species, especially for single 1 μm diameter particles, the identification can be difficult because each material may contribute for such a small fraction of the mass that the relevant peak is below a noise limit (Doughty and Hill, 2020). Furthermore, SEM equipped with an Energy- Dispersive X-ray (EDX) detector has proven to be a powerful technique to investigate the size and the elemental composition and characterize a range of atmospheric aerosol samples (Morillas et al., 2018; Sobanska et al., 2014).

In other research, many PM components have been found employing both Raman spectroscopy and SEM-EDX: silicates and aluminosilicates, carbonates, sulfate and nitrate salts, iron oxides and carbon with D/G band (Correa-Ochoa et al., 2023; Doughty and Hill, 2020; Li et al., 2023; Morillas et al., 2019, 2018).

The use of both RS and SEM-EDX techniques for the investigation of PM samples has already been used in urban areas in industrial and residential contexts (Godoi et al., 2006; González et al., 2018; Sobanska et al., 2014; Stefaniak et al., 2009). SEM microscopy can provide substantial information about the morphology associated with the formation and transportation processes of single particles of PM. The shape of the particle can vary greatly: from flocculent and spherical shape to regular crystalline and irregular shape (Li et al., 2023).

The meteorological parameters are crucial in influencing the concentration of pollutants in the atmosphere (Cheng et al., 2019). Meteorological factors like temperature, wind speed and direction, atmospheric stability, and humidity can significantly impact the

dispersion, transport, and, ultimately the concentration of pollutants in the atmosphere. Furthermore, the terrain of an area also exerts an influence on the concentration (Gohm et al., 2009). For example, valleys and basins can trap pollutants, leading to higher concentrations in those areas. Additionally, the presence of mountains or hills can influence local wind patterns, causing pollutants to accumulate in specific areas. The complex interaction between terrain features and meteorological factors can create microclimates that further impact pollutant concentration (Cheng et al., 2019; Giovannini et al., 2020).

The present study focuses on the air quality in the northern Italian region of Piedmont and its capital, Turin. Five air quality monitoring stations have collected samples over two years from five locations, each representing varying PM quantity and composition based on different sources. This study innovatively displays how PM_{10} composition can simultaneously change in various locations at the same time and in the same location over time, showing how PM composition varies spatially and temporally across the region by incorporating meteorological parameters and terrain features in the analysis. It identifies distinct geographic characteristics, seasonal variations in chemical composition, and diverse PM sources, enhancing the understanding of air pollution's complexity in the region. This offers valuable insight for policymakers and environmental agencies to develop targeted measures for improving air quality and public health.

Moreover, the use of RS and SEM-EDX for the comprehensive characterization of PM10 in the Piedmont region and the city of Turin represents an innovative approach to understanding atmospheric aerosols' different sources and characteristics. The resulting relative abundance of PM from the classification made by Raman presents a new approach to displaying the result. Other researchers typically exclusively list the numerous compounds recognized (Doughty and Hill, 2020; González et al., 2018; Liang et al., 2022; Morillas et al., 2018; Sobanska et al., 2014; Stefaniak et al., 2009) while this study aims to also classify PM to evaluate the share of the components change among the various samplings. Furthermore, a statistical analysis was conducted to determine the appropriate sample size of particles to be analyzed to obtain a statistically meaningful and representative sample.

Also, combining RS and SEM-EDX, provides complementary information about the chemical composition, elemental composition size distribution, and shape of PM_{10} particles. Furthermore, where necessary, the two techniques have been used to collect both Raman and EDX spectra from the same particle to confirm the classification or further investigate the elemental composition of the particle.

2. Materials and methods

2.1. PM sampling locations

2.1.1. Turin and Piedmont

The Piedmont region includes the Po Valley on the eastern side and the Alps on the other side. The Po Valley is one of the most polluted areas in Europe where the European Commission air quality standards are unmet for PM_{10}, NO_2, and O_3 (ARPA Piemonte - Dipartimento Rischi Naturali e Ambientali, 2024). This area is characterized by high primary anthropogenic emissions both from a total population of about 20 million and from a substantial share of the Italian industry (Bo et al., 2020; Finardi et al., 2014).

From an orographic perspective, the Po Valley is bounded by the Adriatic Sea on the eastern side, the Apennines on the southern side, and the Alps on the western and northern sides (Finardi et al., 2014),

enhancing the accumulation of particles in the valley. It is also characterized by a low wind speed, especially in winter, when the average is 1.5 ms^{-1} (ARPA Emilia-Romagna, 2013). During winter, temperature inversions are increasingly frequent causing stagnant atmospheric conditions reducing the vertical dispersion ventilation into the free troposphere (Caserini et al., 2017; Pernigotti et al., 2012). Therefore, the combination of atmospheric stability, low precipitation, and slow ventilation conditions promotes the formation of secondary pollutants due to the high persistence in the air of gaseous precursors (Bo et al., 2020).

Additionally, the Piedmontese capital, Turin, is in dramatic air pollution conditions due to the local emissions and relevant background emissions coming from the Po Valley (Bo et al., 2020). The city is a high-density urban and industrial center and it is surrounded by the Alps in the northwest and the "Collina Torinese" in the southeast creating an even worse unfavorable orographic context for pollution dilution (Pernigotti et al., 2012). During the winter months, the Turin area is subjected to the formation of deep nocturnal thermal inversions, which cause a problematic air pollution condition (Cassardo et al., 2002). All air quality stations in this city register a PM$_{10}$ concentration higher than the daily limit value of 50 μg/m^3 for more than the 35 exceeding days allowed by the European Union Directive 2008/50/EC. In particular, in the year 2022, all the Turin air quality monitoring stations registered a number of exceeding days higher than the law limit, almost doubled for the traffic stations (Città metropolitana di Torino – Dipartimento Ambiente e Vigilanza ambientale et al., 2023). The same European directive also indicates an average annual limit of PM$_{10}$ concentration of 40 μg/m which is almost always met in recent years in Turin.

2.1.2. Air quality monitoring station

Five air quality monitoring stations of the Regional Agency for the Protection of the Environment (Arpa Piemonte) in the northern Italian region of Piedmont are considered in this study. They are all placed in different orographic and pollution contexts (Fig. 1).

The stations of TO-Rebaudengo (TO-R) and TO-Lingotto (TO-L) are located in the center of the metropolitan city of Turin while the other stations (Oulx, Ceresole Reale, and Cavallermaggiore) are in the suburban or rural areas (Table 1).
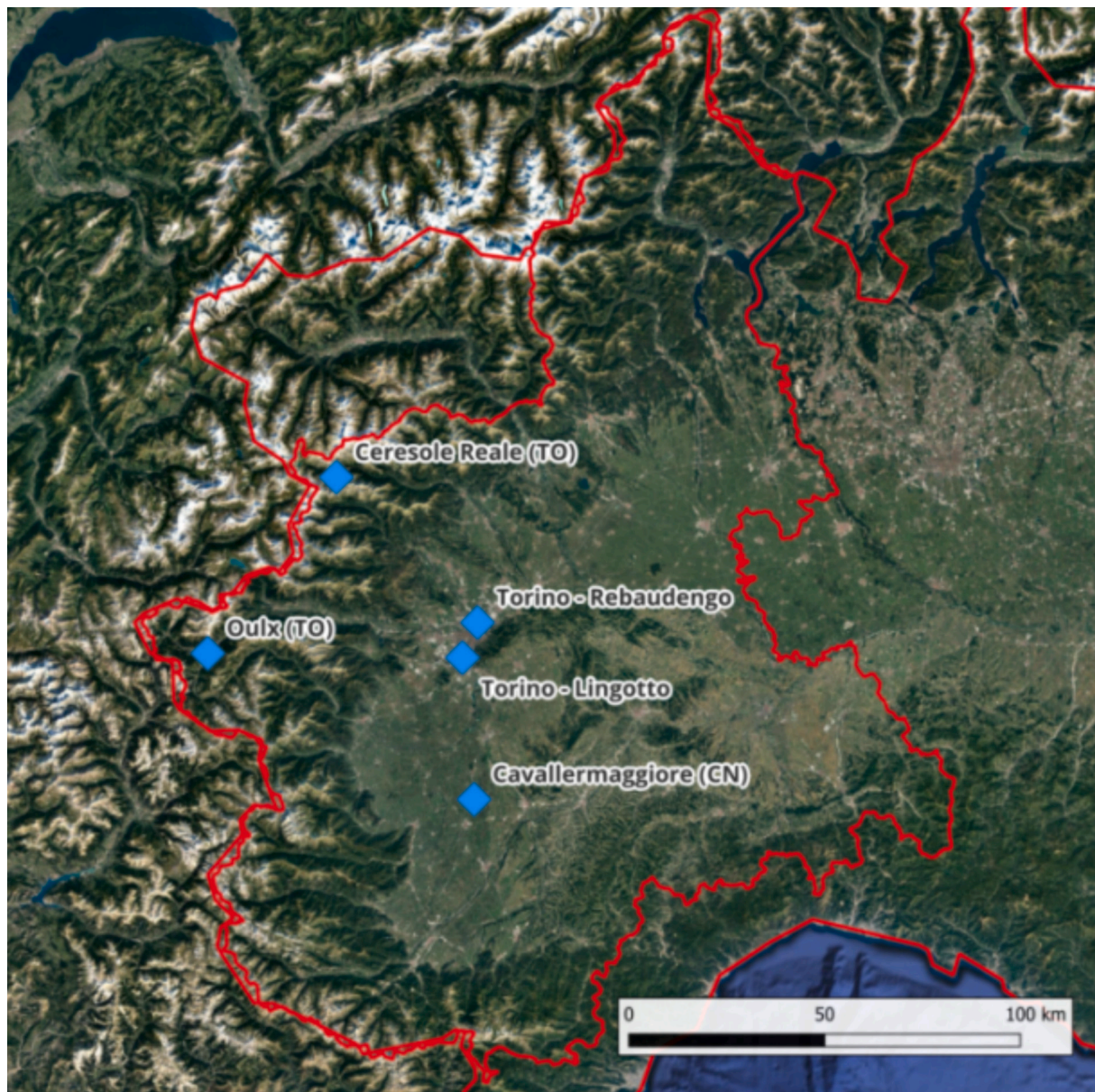

Fig. 1. Five different sampling locations in Piedmont (Italy).

Table 1

Characterization of the sampling location.

Station	Station ID	Coordinates UTM (WGS84)	Characteristic	Emission
TO – Rebaudengo	TO –RE	X: 397426 Y: 4995512	Urban Traffic	Industrial / Residential
TO – Lingotto	TO-L	X: 393640 Y: 4986786	Urban Background	Industrial / Residential
Oulx	CAV	X: 329634 Y: 4989307	Sub-Urban Traffic	Residential
Ceresole Reale	OULX	X: 362750 Y: 5032242	Rural Background	Natural
Cavallermaggiore	CER	X: 395846 Y: 4950945	Sub-Urban Background	Residential/ Agriculture

TO-R station is located in "Piazza Conti di Rebaudengo" near a busy intersection where it has been estimated that about 20,000 vehicles pass a day of which 20 % are diesel heavy trucks. TO-L station is located in a little park called "Parco di Vittorio" at least 50 m away from any source but relatively close to the Lingotto rail station. They are both near industrial and residential emissions, but because of the different context, TO-R station is classified as "Urban Traffic" while TO-L station as "Urban Background" meaning that is more suitable to evaluate the mean exposure to the population. Even if there is a slight decrease in the mean daily PM concentration and the exceedance days of both stations, they report problematic pollution conditions. In particular, in the year 2022 PM_{10} annual value was 34 μg/m^3 for the TO-L station and 37 μg/m^3 for the TO-R station, just below the limit of 40 μg/m3 and far away from the WHO air quality guideline of 15 μg/m^3. In the last decade for both stations, the days with PM_{10} daily value higher than 50 μg/m^3 were well above the permitted value of 35 (Città metropolitana di Torino – Dipartimento Ambiente e Vigilanza ambientale et al., 2023); especially for TO-R station. The different values of the annual average value of NO_2 highlight the difference in the kind of station. In 2022, the average value for TO-L was 31 μg/m3, while for TO-R it was 48 μg/m3 due to the more intense vehicular traffic (Città metropolitana di Torino – Dipartimento Ambiente e Vigilanza ambientale et al., 2023).

The air quality monitoring station of Oulx is located near a state road in a residential area in the municipality of Oulx, which has a population of about 3000 people in the Alps. The air quality station is placed near a state road, and it is classified as a "Sub-Urban Traffic" station, and the values it provides always respect the law limit.

In an almost pristine context, the Ceresole Reale station is situated in the Alps near the dam and the lake "Ceresole Reale". The annual value of PM_{10} is well below the annual law limit and also the WHO air quality guideline of 15 μg/m^3 (ARPA Piemonte - Dipartimento Rischi Naturali e Ambientali, 2023). The station is the Rural Background of the whole region, and the emissions are predominantly from natural sources. The station elevation is higher than the winter mixing layer height, allowing a low value of PM in the cold period which can be high only during Saharan dust transport. During summer, the mixing layer height reaches the altitude of the station causing an increase in the concentration of PM_{10} (Città metropolitana di Torino – Dipartimento Ambiente e Vigilanza ambientale et al., 2022).

The station of Cavallermaggiore is in the corresponding city in the Cuneo province, in the western corner of the Po Valley, with about 5500 inhabitants, which is only monitored from 2021. The air quality condition is considerably influenced by the diffuse stagnant pollution of the Po Valley, which is even more enhanced than the nearby bigger city of Cuneo. The station is classified as a sub-urban background; hence the contribution of local emissions like traffic is not very relevant. In 2022 the daily value of PM_{10} was 32 μg/m^3 and the exceedance days 40 (ARPA Piemonte - Dipartimento Rischi Naturali e Ambientali, 2023) which represents properly the problematic pollution condition even in the small cities in the Po Valley (PM_{10} critic level). The surrounding area/region is also greatly influenced by intensive Zootechnics activities

that generate significant emissions of ammonia. Furthermore, the Cuneo province has the most biogas power plants in Piedmont which considerably contributes to air pollution, specifically, with high emission of nitrogen oxides. They are both precursors of fine secondary particulate matter.

2.2. PM sampling

PM sampling was performed using the Sentinel PM module combined with the Skypost HV atmospheric sampler which allows for the automatic and sequential collection of atmospheric particulate matter on the filter (EN 12341:2023, n.d.). A 47 mm diameter PTFE membrane filter (pore size 2.0 μm) was used to collect the PM. An average airflow of 38.3 l min $^{-1}$ passed through a pickup omnidirectional head screwed on a PM_{10} impactor that allows the filtration of particles with a diameter smaller than 10 μm. Fourteen different representative measurements were carried out from February 2022 to June 2023 (Table 2).

The sampling duration has been chosen based on the filter's readability and the acquisition of a representative sample. The two used durations are 12 h and 24 h. The primary factor affecting the PM sampling time is the quantity of deposited particles related to PM value. In sub-urban and rural environments the daily value of PM is generally lower; hence, a sampling time of 24 h is employed. For urban context (TO-L and TO-R), a 24 h collection can be problematic if the value of PM_{10} is high, so generally, two samples of 12 h and 24 h are scheduled beforehand, and afterward, the more readable sample is analyzed. For the Turin measurements, it is essential to highlight that the mean value of PM_{10} in winter (October–March) is about double the value in summer (April – September) (Città metropolitana di Torino – Dipartimento Ambiente e Vigilanza ambientale et al., 2022). The sampling durations are shown in Table 2.

2.3. Raman spectroscopy

An inVia Raman spectrophotometer (Renishaw, New Mills, UK) was used for the measurements, coupled to a LEICA microscope. A 532 nm diode-pumped solid-state (DPSS) laser with a nominal power of 50 mW was employed. The data acquisition was done using Renishaw's Wire 5.6 software package (New Mills, UK). Depending on the response of the filter, laser powers in the range from 50 to 500 μW provided an adequate signal to noise. The lower end of this range was employed in most cases to prevent excessive sample heating. The acquisition time (15–20 s) and number of accumulations (4–5) were also optimized according to the filter to improve the signal-to-noise ratio. Before use, the Raman spectrophotometer was calibrated using the silicon wafer 520.7 cm^{-1} peak. Particles with a geometric size between 1 μm and 10 μm were selected stochastically in different areas and analyzed in a spectral map mode. Raman bands were assigned through the built-in Renishaw spectra library as well as with the RRUFF open database (Lafuente et al., 2015). If the result is not clear the same particle has been analyzed with SEM-EDX apparatus to obtain further information.

2.3.1. Common PM component found by Raman spectroscopy

RS identified the main components in PM as carbonaceous material, nitrate and sulfate salts, carbonates, iron oxide, and titanium oxide. The most common compound found in the PM by Raman spectroscopy is the carbonaceous material defined by the presence of D (1360 cm^{-1}) and G bands (1580 cm^{-1}) (Doughty and Hill, 2020). These carbonaceous materials can include material defined as soot, coal dust, graphitic carbon, humic substances, and most importantly Black Carbon (BC). Several studies have been performed to correlate the shape of the G and D bands to obtain information on the type of fuel the fuel/oxygen ratio, and the combustion temperature using different excitation wavelength (Russo and Ciajolo, 2015; Sadezky et al., 2005), deconvolution (Ge et al., 2019; Ivleva et al., 2007; Knauer et al., 2009; Sadezky et al., 2005; Severo et al., 2021) or statistical approaches (Feng et al., 2019; Marina-Montes

Table 2
Sampling timetable for the five locations with sampling duration.

	February '22	March '22	May '22	September '22	February '23	March '23	June '23
TO –RE	12 h			12 h	12 h		24 h
TO-L		12 h			12 h		
CAV			12 h		24 h	17 h	24 h
OULX	24 h				24 h		
CER					24 h		24 h

et al., 2022).

A common compound found in PM_{10} can be biological material such as pollen, pieces of trees, shrubs, grasses, and weeds. Even if those materials have been analyzed by Raman spectroscopy, there is currently no complete and comprehensive database of Raman spectra (Félix-Rivera and Hernández-Rivera, 2012; Ivleva et al., 2005; Schulte et al., 2008). Hence, the identification of this PM component can be challenging.

Secondary inorganic aerosols (SIA) represent a significant fraction of fine PM and can be easily identified by RS (Correa-Ochoa et al., 2023; Morillas et al., 2018; Vargas Jentzsch et al., 2013; Zapata and García-Ruiz, 2018) under the category of nitrate, sulfate, and carbonate. For sulfate salt the strongest band is associated with the SO_4^{2-} ion that has four normal modes at 981 cm^{-1} ($\nu1$), 451 cm^{-1} ($\nu2$), 1104 cm^{-1} ($\nu3$), 613 cm^{-1} ($\nu4$), while for the nitrate salt are 1049 cm^{-1} ($\nu1$), 830 cm^{-1} ($\nu2$), 1355 cm^{-1} ($\nu3$), 690 cm^{-1} ($\nu4$) (Correa-Ochoa et al., 2023). It is important to highlight that changes in peak patterns may arise due to various factors, including the potential presence of mixed salts (Vargas Jentzsch et al., 2013; Wang et al., 2021; Zapata and García-Ruiz, 2018). The different compositions and concentrations of diverse kinds of nitrate and sulfate salt depend on many factors: atmospheric ammonia availability, atmospheric composition, meteorological conditions (especially temperature and humidity), and others (Jiang et al., 2017; Le et al., 2020; Lin, 2004). It has been reported that a large share of the composition of $PM_{2.5}$ is ammonium sulfate and ammonium nitrate from the oxidation of ammonia from nitric acid and sulfuric acid (Cesari et al., 2018). Furthermore, other kinds of nitrate and sulfate salt can be found according to different reactions and ion availability: sodium nitrate, calcium nitrate, potassium nitrate, sodium sulfate, and others.

Carbonates, such as $CaCO_3$, can be recognized by RS by its peak at 1432, 1088, 714, 283, and 156 cm^{-1}. The presence of calcite can be correlated with suspended dust or the erosion of calcareous or siliceous rocks from the surrounding environment (Morillas et al., 2016). Furthermore, an anthropogenic origin can be the combustion of biomass, especially if the combustion temperature does not reach 500 °C (Cheah and Ramli, 2011). It has been reported that iron oxide has been found in particular matter as hematite, magnetite, or lepidocrocite (γ-FeO(OH)) (Catelani et al., 2014; Doughty and Hill, 2020; Morillas et al., 2019).

Iron oxides (Fe_2O_3 and Fe_3O_4) can be derived from anthropogenic sources such as brake wear debris (Peikertová et al., 2012) or from natural sources. It has been reported that brake wear debris is often coated with a film of nanosized carbon black particles coming from the oxidation and thermal decomposition of organic compound from the original brake (Kukutschová et al., 2011).

Some studies have reported the presence of titanium oxide in PM in different forms: brookite (γ-TiO_2$), rutile ($\alpha$-TiO_2$), and anatase (β-TiO_2$) (Catelani et al., 2014; Morillas et al., 2019; Sobanska et al., 2014).

Among the crustal elements there are silicates quartz, feldspars (plagioclase and orthoclase), pyroxenes, and rarely garnets have been identified (Catelani et al., 2014; Laskin et al., 2005).

2.4. Scanning electron microscope and energy dispersive spectroscopy (SEM-EDX) integrated technique

The PM samples were placed on an aluminum pin stub covered in carbon conductive tape following the Raman measurement. Then the samples are coated with a 5 nm film by sputtering using a Quorum Q150R S sputter coater (Quorum, Judges House, Lewes Road, Laughton, East Sussex., United Kingdom). A Quanta Inspect 200LV microscope (Fei Company, Hillsboro, OR, USA) combined with an EDX detector (EDAX (Ametek Inc.), Mahwah, NJ, USA) was used to perform the SEM-EDX measurements. Using an acceleration voltage of 20 kV, and a 10 mm working distance, SEM images were acquired under high vacuum conditions. On the contrary, the chosen particle's EDX spectra were obtained using an acceleration voltage of 7.5–10-12 kV.

3. Results and discussion

3.1. Statistical analysis for optimizing PM particle number

A statistical analysis was conducted to obtain a statistically adequate number of particles to provide representative results for each sampling. The PM sample collected in the Cavallermaggiore station was utilized to perform the analysis. A total of 250 Raman spectra has been collected and, according to the Raman bands, assigned to the following classes: Carbon, nitrate salts, sulfate salts, silicate, iron oxide, and titanium oxide.

Groups of particles with increasing numerosity are randomly extracted from the total number of particles. The numerosity of the particle groups considered increases from 10 to 250 with a step size of 5. For each group, the percentages of the chemical compounds are then calculated. This process is replicated for 10,000 iterations to allow the calculation of the mean and standard deviation of the percentages of compounds as the numerosity increases. The relative standard deviation trend (Fig. 2) shows a descending trend for all classes fitted with a 7th-degree polynomial function. The carbon class has the most significant variability. Considering a threshold for the relative standard deviation of 0.05 for the carbon class yields a sampling value of about 100. Considering a safety margin, a value of 140 is regarded as acceptable to represent each sampling statistically.

3.2. Class assignment

Approximately 2000 Raman spectra were collected from the 14 samples examined in this study. The relevant literature, in addition to the RRUFF database, that was referenced to identify each chemical species is provided in Table 3.

Carbon particles can cover other particles, and for this reason, it is present in most spectra. For classification purposes, if a spectrum indicated several responses including amorphous carbon, it was designated to consider only the non-carbon response. The A spectra (Fig. 3) represent the typical shape of the carbon spectra with two broad bands: the D band (1360 cm^{-1}) and the G band (1580 cm^{-1}). This response is typical of soot, coal dust, and most importantly Black Carbon (BC).

Some collected spectra could correspond to pollen (Fig. 3B). They show some peaks that can characterize organic material as shown in other studies (Guedes et al., 2014; Kenđel and Zimmermann, 2020; Zimmermann, 2010). To confirm this theory SEM images show the characteristic aesthetical appearance of pollen; additionally, EDX analysis confirms the almost exclusive presence of C and O (Fig. 4).

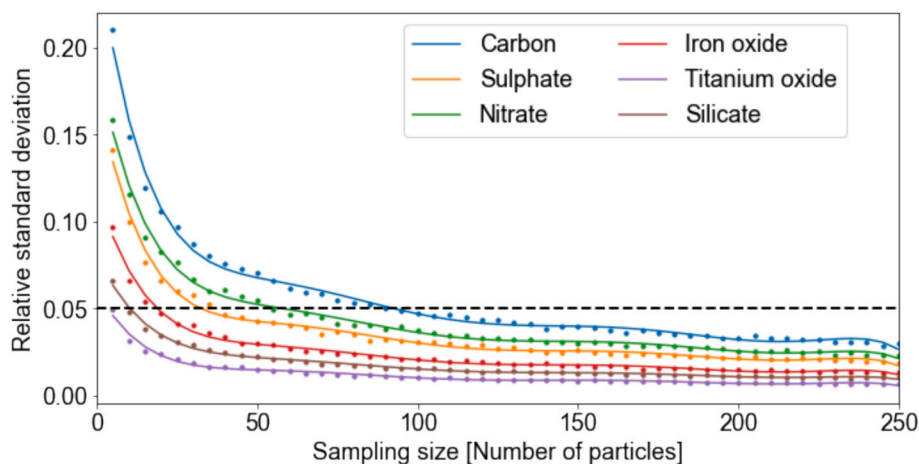Different kinds of nitrate have been encountered: calcium nitrate,

Fig. 2. Trend of the relative standard deviation according to the different compound classes.

Table 3

Main Raman peaks in atmospheric PM_{10}.

Species assigned to	Raman peak (cm − 1)	References
Soot	1300 (D), 1600 (G)	(Feng et al., 2019)
$NaNO_3$	1067,725	(Wang et al., 2021)
NH_4NO_3	1046, 717	(Wang et al., 2021)
KNO_3	1050, 715	(Sun et al., 2019)
$Ca(NO_3)_2$ droplet	1051, 720	(Wang et al., 2021)
$CaSO_4$	1016, 490	(Sun et al., 2019)
$(NH_4)SO_4$	976, 451, 621	(Wang et al., 2021)
$CaCO3$	712, 1082	(Li et al., 2023)
$CaMg(CO3)_2$	1098, 299, 1441	(Wang et al., 2021)
Fe_3O_4 (Hematite)	292, 497, 613	(Morillas et al., 2019)
Fe_2O_3 (Magnetite)	667	(Morillas et al., 2019)
α-TiO_2 (Rutile)	447, 612	(Mazza et al., 2007)
β-TiO_2 (Anatase)	144	(Mazza et al., 2007)
SiO_2	463, 207	(Sun et al., 2019)
Graphite	1600 (G)	(Feng et al., 2019)

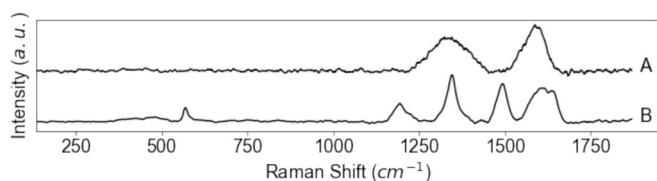**Fig. 4.** SEM images of pollen and their corresponding EDX spectra.

Fig. 3. Raman spectra of Black carbon (A) and pollen (B).

potassium nitrate, sodium nitrate, and ammonium nitrate (Fig. 5, spectra A, B, C). These nitrate species were identified through their characteristic Raman shifts at various wavelengths and further SEM-EDX analysis on arbitrary particles to confirm the Raman results.

Spectrum A represents ammonium nitrate, which forms as a result of a complex process influenced by various factors in particulate matter. Studies have shown that the presence of ammonium in dust particles containing soil organic matter contributes to the formation, along with high concentrations of particulate nitrate in ammonium-poor samples indicating the role of ammonium in nitrate formation (Stelson et al., 1979). Additionally, precursor emissions such as ammonia and nitric acid also play a crucial role (Stelson et al., 1979). Spectrum B represents Calcium and potassium nitrate. The peaks of the two salts, depending on the degree of hydration, show peaks in the same Raman shift range, but arbitrary EDX analyses of these particles revealed the presence of calcium rather than potassium. Calcium nitrate particles can be produced by a heterogeneous reaction of calcium carbonate present in the PM with gaseous nitric acid (Laskin et al., 2005). The spectrum C corresponds to
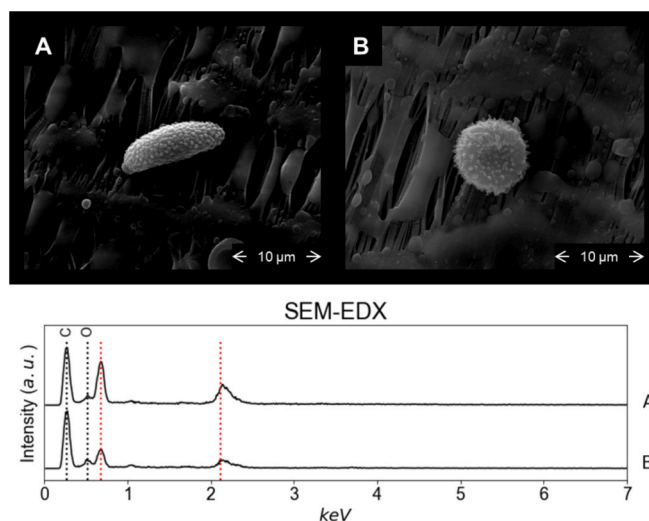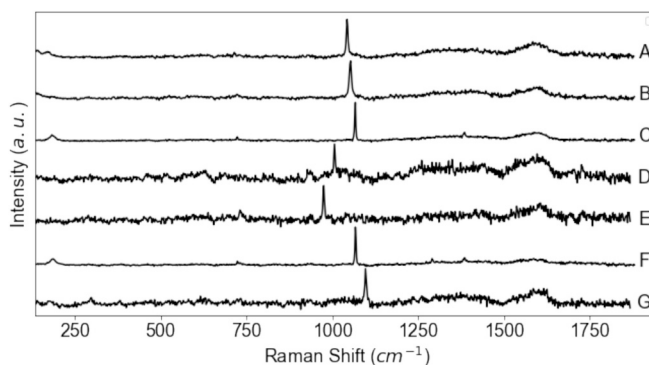

Fig. 5. Raman spectra of nitrate (A, B, C), sulfate (D, E), and carbonates (F, G).

Sodium nitrate (also known as nitratine) which is formed in the atmosphere when salts from marine aerosols react with different nitrogen-containing gases. These reactions occur under diverse conditions of temperature, pressure, and relative humidity (Laskin et al., 2005; Morillas et al., 2018). Raman spectroscopy enables the differentiation and identification of various types of nitrates and sulfates, which are often only quantified as a broader category(Cesari et al., 2018; Seinfeld and Pandis, 2006). This provides a more nuanced understanding of the

specific secondary salts present. However, a limitation for accurate quantification is the particle size, as the analysis focuses on particles larger than 1 μm and may not account for all secondary particles. Furthermore, considering only the relative abundance makes it challenging to determine the absolute concentrations of the different types of secondary salts.

Several varieties of sulfate compounds have been identified, including calcium sulfate, iron sulfate, and ammonium sulfate. Ammonium sulfate is consistently the predominant component, constituting more than 90 % of the composition (Fig. 5E) meanwhile calcium sulfate has been found only rarely (Fig. 5D). The highest concentration of these compounds was observed at the CAV station, which reflects an agricultural environment characterized by extensive use of substances like fertilizers containing precursors to secondary salts such as ammonia.

In this work, two different carbonate species can be identified primarily as calcium carbonate (Fig. 5F) and magnesium calcium carbonate (Fig. 5G); both have been found by other research (Doughty and Hill, 2020; Morillas et al., 2016). The main peak for calcium carbonate is observed at 1086 Raman Shift cm^{-1} is consistent with the RRUFF sample R050128 (while the main peak for magnesium calcium carbonate is found at 1098 Raman Shift cm^{-1}, RRUFF X050115).

The results of the Raman measurements revealed the presence of various types of iron oxide (including hematite, magnetite, and goethite) quartz, titanium oxide and graphite (Fig. 6). In Fig. 6, the A spectra present peaks at 220, 291, 403 and 1300 Raman Shift cm^{-1} (along the D and G band of carbon material) consistent with the spectra from RRUFF database of R040024 of hematite. In Fig. 6, spectrum B shows the characteristic peaks of magnetite (R061111). Some spectra are a combination of both hematite and magnetite (Fig. 6C). Hematite and magnetite are commonly encountered in particulate matter samples across various environmental contexts. (Catelani et al., 2014; Doughty and Hill, 2020; González et al., 2018; Marina-Montes et al., 2022; Morillas et al., 2019, 2016; Sobanska et al., 2014; Wang et al., 2021). Certain spectra exhibit peaks at 293 and 394 Raman Shift cm^{-1} (Fig. 6D), which are indicative of Goethite which has been already found in PM samples(Marina-Montes et al., 2022). This aligns with the data for mineral specimen R120086 in the RRUFF database.

Two distinct varieties of titanium oxide have been discovered. The E spectrum is identified as Anatase and was detected in the winter samples taken from the TO-L station (R070582). Instead, the F spectrum is recognized as Rutile (R110109) and has been identified in multiple samplings. The silicate class is predominantly composed of spectra identified as quartz. The G spectrum collected during the summer sampling in CAV also shows the characteristic peat at quartz at 464 cm^{-1} Raman Shift (R110108). Lastly, a really small amount of graphite (Fig. 6H) has been found in different sampling in urban and suburban contexts.

Fig. 7 shows a portion of the PTFE filter of two distinct samples captured by SEM, along with the corresponding Raman and EDX spectra
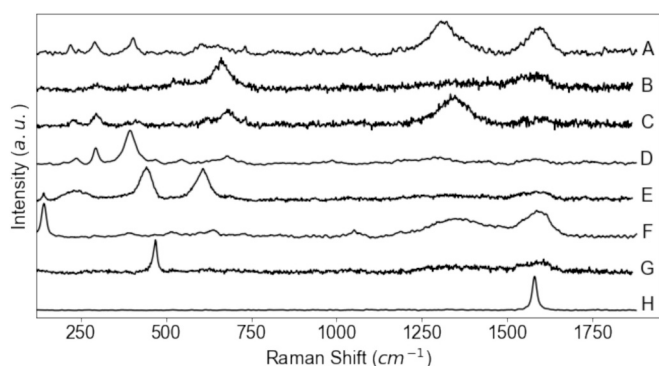
of the indicated PM particle. The dominant components' shapes can be visualized. Nitrate salts (Fig. 7, particle B) and sulfate salts (Fig. 7, particle D) frequently present a regular shape (Fig. 7, particle B); while silicate repeatedly presents an irregular shape (Fig. 7, particle C) as well as iron oxides (Fig. 7, particle E) and calcite (Fig. 7, particle F). Carbon particles (Fig. 7, particle A) exhibit a range of morphologies, including spherical, agglomerated, and organic materials with regular shapes.

SEM-EDX analysis was conducted on the same individual PM particles previously analyzed using Raman spectroscopy (Fig. 7). This complementary analysis also enabled the determination of the elemental composition of PM. The EDX results were then compared to the Raman spectra to validate the identified chemical compound. This innovative combination of techniques allowed for a more comprehensive characterization of the particulate matter, leveraging the strengths of Raman spectroscopy analysis. In particular, SEM-EDX has amply proven to confirm the presence of quartz, iron oxide, sulfate, calcite, and titanium oxide. On the contrary, nitrate and carbon identification has been more challenging because of the PTFE filter interferences (C and F peaks) and the Bremsstrahlung background (N peak).

3.3. PM composition result

After the analysis, for each of the 140 spectra obtained for each sampling, a class was associated with each spectrum to assess the varying percentages of compounds found at different locations and sampling periods. The results are shown in Fig. 8.

Carbon dominates all the sampling, with at least 50 % of the collected spectra being collected in different season, geographic, and emission contexts (Fig. 8). Sulfates characterize the summer period, while the winter period is characterized by nitrates (Fig. 8). The only sampling that reveals a high quantity of both ammonium sulfate and nitrate is the May 2022 sampling of CAV, which straddles the winter and summer seasons It can be argued that the contribution of nitrates in quantitative terms is much greater than the contribution of sulfates, as the quantity of particulate matter during winter is generally higher than during summer. The opposite is true for the CER station, which reports the largest sulfate share of this work.

Looking at the nitrate breakdown results, it can be seen that ammonium nitrate is not the predominant component. For the TO-R station, the contribution of sodium nitrate is very important. The presence of sodium can be traced back to the long-range transport of marine aerosol or from the degradation of sodium chloride used for road deicing and resuspension processes. Further SEM measurements were carried out to confirm this hypothesis, which led to the occasional identification of sodium chloride and a strong presence instead of sodium nitrate (easily recognizable due to its almost cubic form). For the OULX station, in the winter of 2022, the predominant contribution was due to sodium nitrate, while in the winter of 2023 calcium or potassium nitrate as a result of an increased presence of calcite associated with the combustion of biomass from domestic heating; in fact, the SEM-EDX analysis shows a fair amount of sodium chloride. The percentage of ammonium nitrate is similar for the OULX and CER stations, indicating a greater contribution of ammonium ions in the non-urban stations. A greater contribution of ammonium nitrate can be observed for the CAV station, similar to OULX and CER, again confirming the marked presence of ammonium. The percentage change also depends on the geographic context. For the TO-R station, it can be noted that, for the four samplings carried out, the percentage of iron oxides from brake dust is significant and can be attributed to the intense urban traffic. The samplings carried out in the winter of 2022 and 2023 reveal a massive presence of nitrates, mainly from the contribution of sodium nitrates consistent with moderate temperatures. There is also the presence of calcite, mainly in the winter season, which can come from both biomass burning and windblown sedimentary material. The sampling carried out at the TO-L station shows the considerable presence of iron oxides despite its location, which is not near traffic. This percentage can be traced back to the long-

Fig. 6. Raman spectra of iron oxide (A, B, C, D), titanium oxide (E, F), quartz (G), and graphite (H).
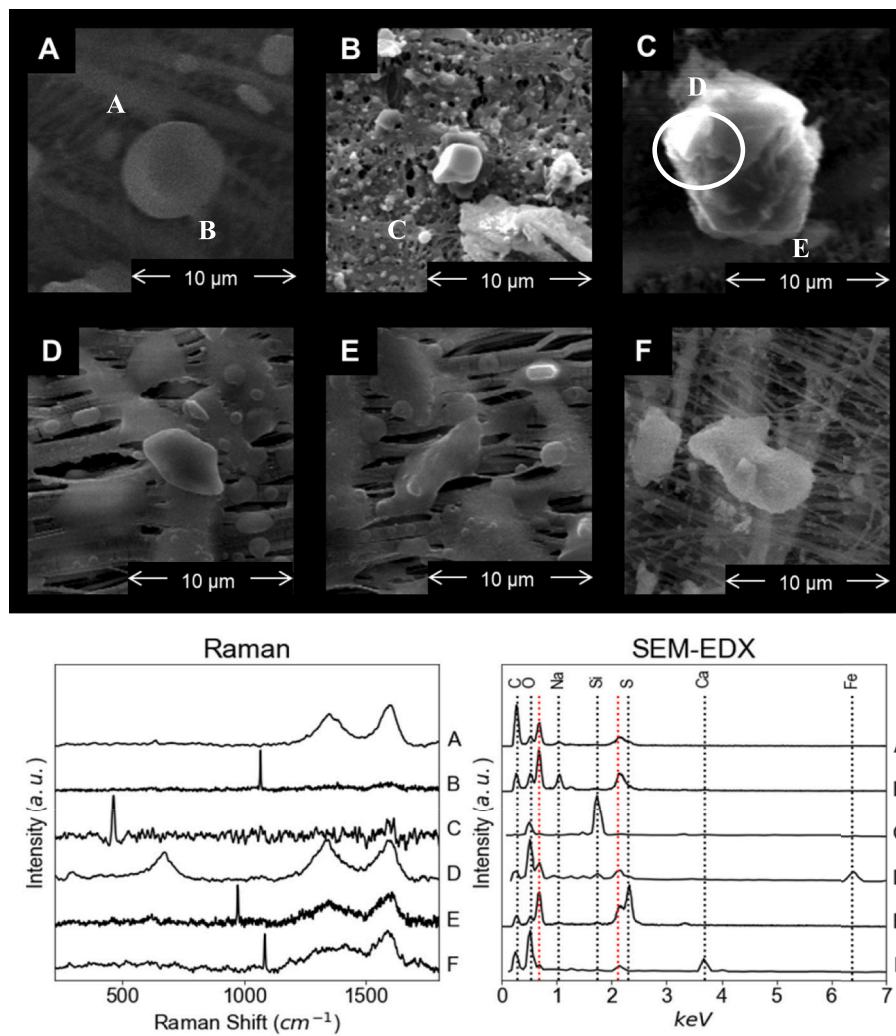
Fig. 7. SEM images of main components: A (Carbon), B (Nitrate), C (Silicate), D (Sulfate), E (Iron oxide), F (Calcite) and their relative Raman spectra (left) and EDX spectra (right).
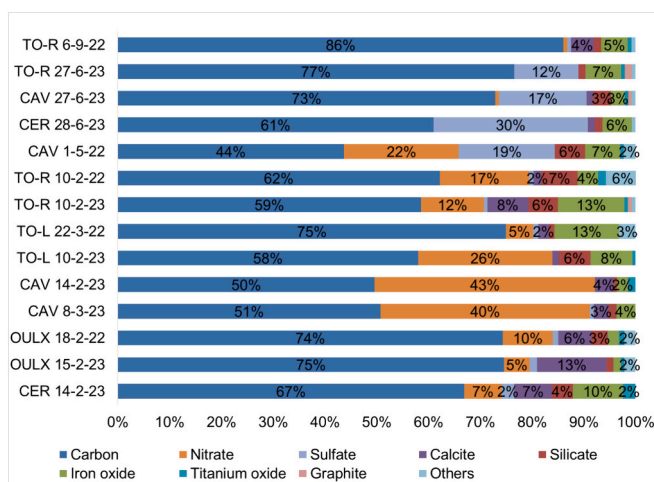
Fig. 8. Share of the PM classes found in all the performed sampling.

range transport of both car brake dust and also from the trains at the Lingotto railway station. The substantial difference in the two samplings carried out lies in the much more significant percentage of nitrates for February 2022 than for March 2023 to be associated with the distinct climatic conditions, including the different average daily temperatures of the two periods considered of 2 and 10 °C respectively. The four samplings at CAV highlight the considerable presence of secondary particulates in the form of nitrates and sulfates. The composition of nitrates found in the winter season varies from that found at the TO-L and TO-R stations due to a higher percentage of ammonium nitrate than sodium nitrate and calcium nitrate. On the other hand, sampling in warmer periods (June and September) shows the consistent presence of sulfates, almost exclusively in the form of ammonium sulfate. Both samplings in OULX were carried out in mid-February in two successive years and produced comparable high carbon values and the presence of calcite and nitrate. The percentage of calcite obtained is one of the highest in this study and can be attributed to the combustion products of biomass, probably from the more extensive use of wood stoves compared to an urban context such as Turin. The two samplings carried out at the CER station report divergent results. The first, carried out in winter 2023, reports the presence of iron oxides, calcite, and nitrate; the second, carried out in June, returns ammonium sulfate and iron oxides. Iron oxides in both samplings emphasize that part of the atmospheric particulate matter does not come from natural sources but also from the contribution of vehicle brake wear that may be produced locally or as a result of long-range transport. Calcite occurs in the winter season and is, therefore, attributable to biomass combustion for domestic heating. The

nitrates found in winter are mainly sodium nitrate and partly ammonium nitrate. The percentage of ammonium sulfate obtained in this study is the highest.

Table 4 shows the result from the sampling during February 2023 in all five air quality monitoring stations. For the TO-R, TO-L, and CAV, the daily value of PM_{10} is critical because it is higher than the law limit of 50 $\mu g/m^3$. There is a consistent amount of nitrate salts for these three stations, especially for the CAV station, which highlights the significant contribution of the formation of secondary PM during the winter months. For the stations of OULX and CER, the contribution of carbon is higher indicating a less important secondary PM contribution. A relevant component along these samplings is the remarkable presence of calcite for the stations of TO-R, OULX, and CER which can be correlated with a more significant amount of domestic heating of biomass or a long transport of crustal dust.

Studying the relative amounts of particulate matter (PM) components is crucial to understanding their health implications. Nitrate salts,

for instance, can cause respiratory issues, cardiovascular problems, and oxidative stress, while sulfate salts, due to their acidic nature, can damage lung tissue and impair lung defense mechanisms (Kampa and Castanas, 2008; Morakinyo et al., 2016) Additionally, mineral dust is known to cause respiratory irritation, silicosis, and infections (Morakinyo et al., 2016). Lastly, carbonaceous particles are associated with respiratory and cardiovascular diseases, inflammation, and increased cancer risk (Bond et al., 2013; Ghio and Huang, 2011; Morakinyo et al., 2016).

4. Conclusion

Raman spectroscopy has proven to provide a rapid and effective methodology for the characterization of particulate matter. However, the results can only be interpreted as the relative proportions of the various components within the total number of analyzed particles, rather than as absolute concentrations. Despite this limitation, the findings are statistically meaningful, as the 140 particles examined constitute a sufficiently robust sample size to allow for comparisons across the different sample sets.

The relative abundance of these compounds varies considerably based on location, emission sources, season, and weather conditions. The predominant components found in the samples include carbon, nitrate salts, sulfate salts, carbonates, and iron oxides. The significant presence of carbon across all samples underscores the need to investigate further and obtain more information. Analyzing the Raman spectra of carbon, specifically the D and G curves and their potential deconvolutions, could provide valuable insights into the type of carbon and its potential emission sources. Notably, significant contributions from nitrate salts are reported in winter, while sulfate salts are more prominent in summer, likely due to the differing temperature and relative humidity conditions. Additionally, the presence of certain particles, such as sodium chloride and sodium nitrate, can be influenced by various factors, including long-range transport of sea salt aerosols, the degradation of road de-icing agents, and specific environmental conditions, such as the absence of rain.

The findings of this study could be useful to specify the principal PM constituent classes, particularly during the winter months when daily particulate matter limits are consistently surpassed, to comply with current air quality regulations and support future regulatory measures in urban and sub-urban areas. Specifically, efforts should focus on reducing carbon emission sources and the precursors to secondary salt formation.

CRediT authorship contribution statement

Lia Drudi: Writing – review & editing, Writing – original draft, Visualization, Validation, Software, Methodology, Investigation, Formal analysis, Data curation. **Matteo Giardino:** Writing – review & editing, Validation, Software, Methodology, Formal analysis. **Marilena Tedone:** Writing – review & editing, Validation, Software, Investigation, Formal analysis. **Andrea Tiano:** Writing – review & editing, Validation, Software, Formal analysis. **Davide Janner:** Writing – review & editing, Conceptualization. **Federica Pognant:** Writing – review & editing, Resources, Conceptualization. **Francesco Matera:** Writing – review & editing, Resources, Conceptualization. **Milena Sacco:** Writing – review & editing, Resources, Methodology. **Luisella Bardi:** Writing – review & editing, Resources, Conceptualization. **Rossana Bellopede:** Writing – review & editing, Supervision, Resources, Project administration, Funding acquisition, Conceptualization.

Declaration of competing interest

The authors declare the following financial interests/personal relationships which may be considered as potential competing interests: Lia Drudi reports financial support was provided by Polytechnic of Turin. If there are other authors, they declare that they have no known

Table 4
Sampling in different locations in February 2023 and daily PM_{10}, temperature, and relative humidity values.

Stations	Monitoring data			Compounds percentages
	PM_{10} ($\mu g/m^3$)	T_{mean} (°C)	HR_{mean} (%)	■ Carbon ■ Silicate ■ Iron oxide ■ Calcite ■ Titanium oxide ■ Nitrate ■ Sulphate ■ Graphite ■ Other
TO – R	59	3	47	Carbon 58%, Silicate 6%, Calcite 13%, Nitrate 8%, Other 12%
TO – L	51	3	47	Carbon 58%, Silicate 6%, Calcite 8%, Nitrate 26%
OULX	16	5	54	Carbon 75%, Calcite 13%, Nitrate 5%
CER	4	2	32	Carbon 67%, Silicate 4%, Calcite 10%, Sulphate 7%, Nitrate 7%, Other 7%
CAV	57	8	57	Carbon 50%, 3%, Nitrate 43%

competing financial interests or personal relationships that could have appeared to influence the work reported in this paper.

Data availability

Data will be made available on request.

Acknowledgment

References

ARPA Emilia-Romagna, 2013. Piano regionale integrato per la qualità dell'aria dell'Emilia- Romagna: quadro conoscitivo.

ARPA Piemonte - Dipartimento Rischi Naturali e Ambientali, 2023. La qualità dell'aria in Piemonte - Relazione sintetica 2022.

ARPA Piemonte - Dipartimento Rischi Naturali e Ambientali, 2024. La qualità dell'aria in Piemonte - Relazione sintetica 2023.

Bo, M., Charvolin-Volta, P., Clerico, M., Nguyen, C.V., Pognant, F., Soulhac, L., Salizzoni, P., 2020. Urban air quality and meteorology on opposite sides of the Alps: the Lyon and Torino case studies. Urban Clim. 34, 100698 https://doi.org/10.1016/j.uclim.2020.100698.

Bond, T.C., Doherty, S.J., Fahey, D.W., Forster, P.M., Berntsen, T., DeAngelo, B.J., Flanner, M.G., Ghan, S., Kärcher, B., Koch, D., Kinne, S., Kondo, Y., Quinn, P.K., Sarofim, M.C., Schultz, M.G., Schulz, M., Venkataraman, C., Zhang, H., Zhang, S., Bellouin, N., Guttikunda, S.K., Hopke, P.K., Jacobson, M.Z., Kaiser, J.W., Klimont, Z., Lohmann, U., Schwarz, J.P., Shindell, D., Storelvmo, T., Warren, S.G., Zender, C.S., 2013. Bounding the role of black carbon in the climate system: a scientific assessment. JGR Atmospheres 118, 5380–5552. https://doi.org/10.1002/jgrd.50171.

Caserini, S., Giani, P., Cacciamani, C., Ozgen, S., Lonati, G., 2017. Influence of climate change on the frequency of daytime temperature inversions and stagnation events in the Po Valley: historical trend and future projections. Atmos. Res. 184, 15–23. https://doi.org/10.1016/j.atmosres.2016.09.018.

Cassardo, C., Forza, R., Manfrin, M., Longhetto, A., Qian, M.W., Richiardone, R., Balsamo, G.P., 2002. The urban meteorological staion of Turin, in: Proc. 11 Th Symposium on Acoustic Remote Sensing. Presented at the 11 th Symposium on Acoustic Remote Sensing, Rome, pp. 311–320.

Catelani, T., Pratesi, G., Zoppi, M., 2014. Raman characterization of ambient airborne soot and associated mineral phases. Aerosol Sci. Tech. 48, 13–21. https://doi.org/10.1080/02786826.2013.847270.

Cesari, D., De Benedetto, G.E., Bonasoni, P., Busetto, M., Dinoi, A., Merico, E., Chirizzi, D., Cristofanelli, P., Donateo, A., Grasso, F.M., Marinoni, A., Pennetta, A., Contini, D., 2018. Seasonal variability of PM2.5 and PM10 composition and sources in an urban background site in southern Italy. Sci. Total Environ. 612, 202–213. https://doi.org/10.1016/j.scitotenv.2017.08.230.

Cheah, C.B., Ramli, M., 2011. The implementation of wood waste ash as a partial cement replacement material in the production of structural grade concrete and mortar: an overview. Resour. Conserv. Recycl. 55, 669–685. https://doi.org/10.1016/j.resconrec.2011.02.002.

Cheng, Q., Li, M., Li, F., Tang, H., 2019. Response of global air pollutant emissions to climate change and its potential effects on human life expectancy loss. Sustainability 11, 3670. https://doi.org/10.3390/su11133670.

Città metropolitana di Torino – Dipartimento Ambiente e Vigilanza ambientale, ARPA Piemonte - Dipartimento Territoriale Piemonte Nord-Ovest, ARPA Piemonte - Dipartimento Rischi Naturali e Ambientali, 2023. Relazione annuale sui dati rilevati dalla rete metropolitana di monitoraggio della qualità dell'aria 2022.

Città metropolitana di Torino – Dipartimento Ambiente e Vigilanza ambientale, ARPA Piemonte - Dipartimento territoriale Piemonte Nord-Ovest, ARPA Piemonte - Dipartimento Rischi Naturali e Ambientali, Università degli studi di Torino, Dipartimento Scienze della Sanità Pubblica e Pediatriche, 2022. Relazione annuale sui dati rilevati dalla rete metropolitana di monitoraggio della qualità dell'aria 2021.

Correa-Ochoa, M.A., Rojas, J., Gómez, L.M., Aguiar, D., Palacio-Tobón, C.A., Colorado, H.A., 2023. Systematic search using the Proknow-C method for the characterization of atmospheric particulate matter using the materials science techniques XRD, FTIR, XRF, and Raman spectroscopy. Sustainability 15, 8504. https://doi.org/10.3390/su15118504.

Doughty, D.C., Hill, S.C., 2020. Raman spectra of atmospheric aerosol particles: clusters and time-series for a 22.5 hr sampling period. J. Quant. Spectrosc. Radiat. Transf. 248, 106907 https://doi.org/10.1016/j.jqsrt.2020.106907.

EN 12341:2023, n.d. Ambient Air. Standard Gravimetric Measurement Method for the Determination of the PM$_{10}$ or PM$_{2.5}$ Mass Concentration of Suspended Particulate Matter. BSI British Standards. doi:https://doi.org/10.3403/30260964.

Estefany, C., Sun, Z., Hong, Z., Du, J., 2023. Raman spectroscopy for profiling physical and chemical properties of atmospheric aerosol particles: a review. Ecotoxicol. Environ. Saf. 249, 114405 https://doi.org/10.1016/j.ecoenv.2022.114405.

Félix-Rivera, H., Hernández-Rivera, S.P., 2012. Raman spectroscopy techniques for the detection of biological samples in suspensions and as aerosol particles: a review. Sens Imaging 13, 1–25. https://doi.org/10.1007/s11220-011-0067-0.

Feng, Y., Liu, L., Yang, Y., Deng, Y., Li, K., Cheng, H., Dong, X., Li, W., Zhang, L., 2019. The application of Raman spectroscopy combined with multivariable analysis on source apportionment of atmospheric black carbon aerosols. Sci. Total Environ. 685, 189–196. https://doi.org/10.1016/j.scitotenv.2019.05.367.

Finardi, S., Silibello, C., D'Allura, A., Radice, P., 2014. Analysis of pollutants exchange between the Po Valley and the surrounding European region. Urban Clim. 10, 682–702. https://doi.org/10.1016/j.uclim.2014.02.002.

Ge, H., Ye, Z., He, R., 2019. Raman spectroscopy of diesel and gasoline engine-out soot using different laser power. J. Environ. Sci. 79, 74–80. https://doi.org/10.1016/j.jes.2018.11.001.

Ghio, A.J., Huang, Y.T., 2011. Role of chemical composition in determining the cardiovascular effects of particles. In: Mills, N.L., Newby, D. (Eds.), Cassee, F.R. Wiley, Cardiovascular Effects of Inhaled Ultrafine and Nanosized Particles, pp. 145–167. https://doi.org/10.1002/9780470910917.ch8.

Giovannini, L., Ferrero, E., Karl, T., Rotach, M.W., Staquet, C., Trini Castelli, S., Zardi, D., 2020. Atmospheric pollutant dispersion over complex terrain: challenges and needs for improving air quality measurements and modeling. Atmosphere 11, 646. https://doi.org/10.3390/atmos11060646.

Godoi, R.H.M., Potgieter-Vermaak, S., De Hoog, J., Kaegi, R., Van Grieken, R., 2006. Substrate selection for optimum qualitative and quantitative single atmospheric particles analysis using nano-manipulation, sequential thin-window electron probe X-ray microanalysis and micro-Raman spectrometry. Spectrochim. Acta B At. Spectrosc. 61, 375–388. https://doi.org/10.1016/j.sab.2006.02.004.

Gohm, A., Harnisch, F., Vergeiner, J., Obleitner, F., Schnitzhofer, R., Hansel, A., Fix, A., Neininger, B., Emeis, S., Schäfer, K., 2009. Air pollution transport in an Alpine Valley: results from airborne and ground-based observations. Boundary-Layer Meteorol 131, 441–463. https://doi.org/10.1007/s10546-009-9371-9.

González, L.T., Longoria-Rodríguez, F.E., Sánchez-Domínguez, M., Leyva-Porras, C., Acuña-Askar, K., Kharissov, B.I., Arizpe-Zapata, A., Alfaro-Barbosa, J.M., 2018. Seasonal variation and chemical composition of particulate matter: a study by XPS, ICP-AES and sequential microanalysis using Raman with SEM/EDS. J. Environ. Sci. 74, 32–49. https://doi.org/10.1016/j.jes.2018.02.002.

Guedes, A., Ribeiro, H., Fernández-González, M., Aira, M.J., Abreu, I., 2014. Pollen Raman spectra database: application to the identification of airborne pollen. Talanta 119, 473–478. https://doi.org/10.1016/j.talanta.2013.11.046.

Ivleva, N.P., Niessner, R., Panne, U., 2005. Characterization and discrimination of pollen by Raman microscopy. Anal. Bioanal. Chem. 381, 261–267. https://doi.org/10.1007/s00216-004-2942-1.

Ivleva, N.P., Messerer, A., Yang, X., Niessner, R., Pöschl, U., 2007. Raman microspectroscopic analysis of changes in the chemical structure and reactivity of soot in a diesel exhaust Aftertreatment model system. Environ. Sci. Technol. 41, 3702–3707. https://doi.org/10.1021/es0612448.

Jiang, N., Guo, Y., Wang, Q., Kang, P., Zhang, R., Tang, X., 2017. Chemical composition characteristics of PM2.5 in three cities in Henan. Central China. Aerosol Air Qual. Res. 17, 2367–2380. https://doi.org/10.4209/aaqr.2016.10.0463.

Kampa, M., Castanas, E., 2008. Human health effects of air pollution. Environ. Pollut. 151, 362–367. https://doi.org/10.1016/j.envpol.2007.06.012.

Kendel, A., Zimmermann, B., 2020. Chemical analysis of pollen by FT-Raman and FTIR spectroscopies. Front. Plant Sci. 11, 352. https://doi.org/10.3389/fpls.2020.00352.

Knauer, M., Schuster, M.E., Su, D., Schlögl, R., Niessner, R., Ivleva, N.P., 2009. Soot structure and reactivity analysis by Raman microspectroscopy, temperature-programmed oxidation, and high-resolution transmission Electron microscopy. J. Phys. Chem. A 113, 13871–13880. https://doi.org/10.1021/jp905639d.

Kukutschová, J., Moravec, P., Tomášek, V., Matějka, V., Smolík, J., Schwarz, J., Seidlerová, J., Šafářová, K., Filip, P., 2011. On airborne nano/micro-sized wear particles released from low-metallic automotive brakes. Environ. Pollut. 159, 998–1006. https://doi.org/10.1016/j.envpol.2010.11.036.

Lafuente, B., Downs, R.T., Yang, H., Stone, N., 2015. 1. The power of databases: The RRUFF project, in: Armbruster, T., Danisi, R.M. (Eds.), Highlights in Mineralogical Crystallography. DE GRUYTER, pp. 1–30. doi:10.1515/9783110417104-003.

Laskin, A., Iedema, M.J., Ichkovich, A., Graber, E.R., Taraniuk, I., Rudich, Y., 2005. Direct observation of completely processed calcium carbonate dust particles. Faraday Discuss. 130, 453. https://doi.org/10.1039/b417366j.

Le, T.-C., Wang, Y.-C., Pui, D.Y.H., Tsai, C.-J., 2020. Characterization of atmospheric PM2.5 inorganic aerosols using the semi-continuous PPWD-PILS-IC system and the ISORROPIA-II. Atmosphere 11, 820. https://doi.org/10.3390/atmos11080820.

Li, D., Yue, W., Gong, T., Gao, P., Zhang, T., Luo, Y., Wang, C., 2023. A comprehensive SERS, SEM and EDX study of individual atmospheric PM2.5 particles in Chengdu, China. Sci. Total Environ. 883, 163668 https://doi.org/10.1016/j.scitotenv.2023.163668.

Liang, Z., Chu, Y., Gen, M., Chan, C.K., 2022. Single-particle Raman spectroscopy for studying physical and chemical processes of atmospheric particles. Atmos. Chem. Phys. 22, 3017–3044. https://doi.org/10.5194/acp-22-3017-2022.

Lin, J., 2004. Characterization of the concentration and distribution of urban submicron (PM1) aerosol particles. Atmos. Environ. 38, 469–475. https://doi.org/10.1016/j.atmosenv.2003.09.056.

Manisalidis, I., Stavropoulou, E., Stavropoulos, A., Bezirtzoglou, E., 2020. Environmental and health impacts of air pollution: a review. Front. Public Health 8, 14. https://doi.org/10.3389/fpubh.2020.00014.

Marina-Montes, C., Pérez-Arribas, L.V., Anzano, J., De Vallejuelo, S.F.-O., Aramendia, J., Gómez-Nubla, L., De Diego, A., Manuel Madariaga, J., Cáceres, J.O., 2022. Characterization of atmospheric aerosols in the Antarctic region using Raman spectroscopy and scanning Electron microscopy. Spectrochim. Acta A Mol. Biomol. Spectrosc. 266, 120452 https://doi.org/10.1016/j.saa.2021.120452.

Mazza, T., Barborini, E., Piseri, P., Milani, P., Cattaneo, D., Li Bassi, A., Bottani, C.E., Ducati, C., 2007. Raman spectroscopy characterization of Ti O 2 rutile nanocrystals. Phys. Rev. B 75, 045416. https://doi.org/10.1103/PhysRevB.75.045416.

Morakinyo, O., Mokgobu, M., Mukhola, M., Hunter, R., 2016. Health outcomes of exposure to biological and chemical components of inhalable and respirable particulate matter. IJERPH 13, 592. https://doi.org/10.3390/ijerph13060592.

Morillas, H., Maguregui, M., García-Florentino, C., Marcaida, I., Madariaga, J.M., 2016. Study of particulate matter from primary/secondary marine aerosol and anthropogenic sources collected by a self-made passive sampler for the evaluation of the dry deposition impact on built heritage. Sci. Total Environ. 550, 285–296. https://doi.org/10.1016/j.scitotenv.2016.01.080.

Morillas, H., Marcaida, I., García-Florentino, C., Maguregui, M., Arana, G., Madariaga, J. M., 2018. Micro-Raman and SEM-EDS analyses to evaluate the nature of salt clusters present in secondary marine aerosol. Sci. Total Environ. 615, 691–697. https://doi.org/10.1016/j.scitotenv.2017.09.299.

Morillas, H., Marcaida, I., Maguregui, M., Upasen, S., Gallego-Cartagena, E., Madariaga, J.M., 2019. Identification of metals and metalloids as hazardous elements in PM2.5 and PM10 collected in a coastal environment affected by diffuse contamination. J. Clean. Prod. 226, 369–378. https://doi.org/10.1016/j.jclepro.2019.04.063.

Peikertová, P., Vaculík, M., Filip, P., Kukutschová, J., 2012. Raman Microspectroscopy as a Tool for Characterization of Brake Wear Debris.

Pernigotti, D., Georgieva, E., Thunis, P., Bessagnet, B., 2012. Impact of meteorology on air quality modeling over the Po valley in northern Italy. Atmos. Environ. 51, 303–310. https://doi.org/10.1016/j.atmosenv.2011.12.059.

Russo, C., Ciajolo, A., 2015. Effect of the flame environment on soot nanostructure inferred by Raman spectroscopy at different excitation wavelengths. Combust. Flame 162, 2431–2441. https://doi.org/10.1016/j.combustflame.2015.02.011.

Sadezky, A., Muckenhuber, H., Grothe, H., Niessner, R., Pöschl, U., 2005. Raman microspectroscopy of soot and related carbonaceous materials: spectral analysis and structural information. Carbon 43, 1731–1742. https://doi.org/10.1016/j.carbon.2005.02.018.

Schulte, F., Lingott, J., Panne, U., Kneipp, J., 2008. Chemical characterization and classification of pollen. Anal. Chem. 80, 9551–9556. https://doi.org/10.1021/ac801791a.

Schwartz, J., 2004. Air Pollution and Children's Health. Pediatrics 113, 1037–1043. https://doi.org/10.1542/peds.113.S3.1037.

Schwarze, P.E., Øvrevik, J., Låg, M., Refsnes, M., Nafstad, P., Hetland, R.B., Dybing, E., 2006. Particulate matter properties and health effects: consistency of epidemiological and toxicological studies. Hum. Exp. Toxicol. 25, 559–579. https://doi.org/10.1177/096032706072520.

Seinfeld, J.H., Pandis, S.N., 2006. From Air Pollution to Climate Change, 2nd ed. John Wiley & Sons.

Severo, L.S., Rodrigues, J.B., Campanelli, D.A., Pereira, V.M., Menezes, J.W., De Menezes, E.W., Valsecchi, C., Vasconcellos, M.A.Z., Armas, L.E.G., 2021. Synthesis and Raman characterization of wood sawdust ash, and wood sawdust ash-derived graphene. Diamond Relat. Mater. 117, 108496 https://doi.org/10.1016/j.diamond.2021.108496.

Sobanska, S., Falgayrac, G., Rimetz-Planchon, J., Perdrix, E., Brémard, C., Barbillat, J., 2014. Resolving the internal structure of individual atmospheric aerosol particle by the combination of atomic force microscopy, ESEM–EDX, Raman and ToF–SIMS imaging. Microchem. J. 114, 89–98. https://doi.org/10.1016/j.microc.2013.12.007.

Stefaniak, E.A., Buczynska, A., Novakovic, V., Kuduk, R., Grieken, R.V., 2009. Determination of chemical composition of individual airborne particles by SEM/EDX and micro-Raman spectrometry: a review. J. Phys. Conf. Ser. 162, 012019 https://doi.org/10.1088/1742-6596/162/1/012019.

Stelson, A.W., Friedlander, S.K., Seinfeld, J.H., 1979. A note on the equilibrium relationship between ammonia and nitric acid and particulate ammonium nitrate. Atmos. Environ. 1967 (13), 369–371. https://doi.org/10.1016/0004-6981(79)90293-2.

Sun, Z., Duan, F., He, K., Du, J., Yang, L., Li, H., Ma, T., Yang, S., 2019. Physicochemical analysis of individual atmospheric fine particles based on effective surface-enhanced Raman spectroscopy. J. Environ. Sci. 75, 388–395. https://doi.org/10.1016/j.jes.2018.06.006.

Vargas Jentzsch, P., Kampe, B., Ciobotă, V., Rösch, P., Popp, J., 2013. Inorganic salts in atmospheric particulate matter: Raman spectroscopy as an analytical tool. Spectrochim. Acta A Mol. Biomol. Spectrosc. 115, 697–708. https://doi.org/10.1016/j.saa.2013.06.085.

Wang, M., Zheng, N., Zhao, D., Shang, J., Zhu, T., 2021. Using Micro-Raman spectroscopy to investigate chemical composition, mixing states, and heterogeneous reactions of individual atmospheric particles. Environ. Sci. Technol. 55, 10243–10254. https://doi.org/10.1021/acs.est.1c01242.

Yang, Y., Pun, V.C., Sun, S., Lin, H., Mason, T.G., Qiu, H., 2018. Particulate matter components and health: a literature review on exposure assessment. J Public Health Emerg 2, 14. https://doi.org/10.21037/jphe.2018.03.03.

Zapata, F., García-Ruiz, C., 2018. The discrimination of 72 nitrate, chlorate and perchlorate salts using IR and Raman spectroscopy. Spectrochim. Acta A Mol. Biomol. Spectrosc. 189, 535–542. https://doi.org/10.1016/j.saa.2017.08.058.

Zimmermann, B., 2010. Characterization of pollen by vibrational spectroscopy. Appl. Spectrosc. 64, 1364–1373. https://doi.org/10.1366/000370210793561664.